

Including massive neutrinos in thermal Sunyaev Zeldovich power spectrum and cluster counts analyses

Boris Bolliet¹, Thejs Brinckmann^{2,3}, Jens Chluba¹, Julien Lesgourgues³

¹*Jodrell Bank Centre for Astrophysics, School of Physics and Astronomy, The University of Manchester, Manchester, M13 9PL, U.K.*

²*C.N. Yang Institute for Theoretical Physics and Department of Physics & Astronomy, Stony Brook University, Stony Brook, NY 11794, USA*

³*Institute for Theoretical Particle Physics and Cosmology (TTK), RWTH Aachen University, D-52056 Aachen, Germany*

16 June 2022

ABSTRACT

We consistently include the effect of massive neutrinos in the thermal Sunyaev Zeldovich (SZ) power spectrum and cluster counts analyses, highlighting subtle dependencies on the parameterisation and data combination. In Λ CDM, with an X-ray mass bias corresponding the expected hydrostatic mass bias, i.e., $b \simeq 0.2$, our constraints from Planck SZ data are consistent with the latest results from SPT, DES-Y1 and KiDS+VIKING-450. In $\nu\Lambda$ CDM, without prior information on b , our joint analyses of Planck SZ with Planck 2015 primary CMB yield a small improvement on the total neutrino mass bound compared to the Planck 2015 primary CMB constraint, as well as $(1 - b) = 0.64 \pm 0.04$ (68% CL). For forecasts, we find that a combination of a mock cosmic variance limited SZ power spectrum with primary CMB and BAO can improve the uncertainty on the total neutrino mass by 14% with respect to CMB combined with BAO. This requires masking the heaviest clusters and probing the small-scale SZ power spectrum up to multipoles of $\ell_{\text{max}} = 10^4$. For a future competitive measurement of the total neutrino mass using CMB and the SZ power spectrum, but excluding BAO and lensing power spectrum, we find that a 1% precision on the mass calibration of clusters is needed. Although SZ power spectrum-based measurements of the neutrino masses are challenging, we find that the SZ power spectrum can be used to tightly constrain intra-cluster medium properties.

Key words: cosmological parameters – cosmology: observations – cosmology: theory – galaxies: clusters: intra-cluster medium.

1 INTRODUCTION

Observationally, the structure of the present Universe appears as a web of cosmic voids and dense filaments filled with baryonic matter and a cold dark matter (CDM). At the crossroads of these filaments lie clusters of several hundreds of galaxies, constituting the largest known gravitationally bound objects. In the past decades, the properties of galaxy clusters have been determined using several techniques including weak lensing, optical, X-ray and Sunyaev Zeldovich (SZ) surveys (see, e.g., Burenin et al. 2007; Vikhlinin et al. 2009; Planck Collaboration 2016d; Hilton et al. 2018; de Haan et al. 2016; Ruppin et al. 2018). Galaxy clusters have a typical mass of a few $10^{14} M_{\odot}$. About ten percents of the mass is a hot electron gas with temperatures reaching $T \approx 5\text{--}10$ keV, while galaxies themselves are responsible for only about one percent of the total mass. The remainder of the mass is made of CDM. On scales smaller than the cluster size, observations and simulations have shown that the structure of the

intra-cluster medium (ICM) is well described by a Navarro-Frenk-White (NFW) profile for the CDM density (Navarro et al. 1996) that translates into a generalised NFW pressure profile for the hot gas of electrons (Nagai et al. 2007b; Arnaud et al. 2010). Since galaxy clusters form in the potential wells created by CDM, their large-scale distribution directly traces the underlying cosmological perturbation field. Therefore, their abundance and spatial distribution provide a powerful cosmological probe and it is crucial to understand how subtle effects, e.g., caused by massive neutrinos, propagate into cluster observables.

Neutrino oscillations experiments show that neutrinos are massive (see, e.g., Kajita 2016; de Salas et al. 2018; Esteban et al. 2019). The three mass states can be arranged in the so-called normal hierarchy, with one mass state significantly larger than the other two, or the inverted hierarchy, where two mass states are significantly larger than the third. Respectively, these configurations imply $\Sigma m_{\nu} \gtrsim 0.06$ eV

and $\Sigma m_\nu \gtrsim 0.1\text{eV}$ for the total neutrino mass. Current constraints from cosmology give $\Sigma m_\nu \lesssim 0.12\text{eV}$ at 95% CL (e.g., [Palanque-Delabrouille et al. 2015](#); [Cuesta et al. 2016](#); [Giusarma et al. 2016](#); [Vagnozzi et al. 2017](#); [Planck Collaboration 2018](#)) combining Cosmic Microwave Background (CMB) and Baryon Acoustic Oscillations (BAO) data in ΛCDM . This translates into upper bounds on the individual neutrino mass states, but the hierarchy is still unknown.

Significant progress have been made in recent years towards understanding neutrino mass effects in cosmology in order to improve upon current constraints (e.g., [Allison et al. 2015](#); [Liu et al. 2016](#); [LoVerde 2016](#); [Archidiacono et al. 2017](#); [Alam et al. 2017](#); [Lorenz et al. 2017](#); [Boyle & Komatsu 2018](#); [Yu et al. 2018](#); [Boyle 2019](#); [Oldengott et al. 2019](#)). A neutrino mass sum measurement is furthermore expected from future large-scale structure and galaxy surveys such as DESI, LSST, Euclid and SKA (e.g. [Audren et al. 2013b](#); [Villaescusa-Navarro et al. 2015](#); [Di Valentino et al. 2018](#); [Calabrese et al. 2017a](#); [Obuljen et al. 2018](#); [Sprenger et al. 2019](#); [Mishra-Sharma et al. 2018](#); [Brinckmann et al. 2019](#)). Aside from determining the neutrino mass hierarchy, a neutrino mass sum detection from cosmology would put lower bounds on the two larger mass states and, in the case of a non-minimal normal hierarchy, a lower bound on the lightest neutrino mass state.¹

The thermal SZ power spectrum probes galaxy clusters on cosmological scales via the SZ effect, a spectral distortion of the CMB radiation spectrum due to the up-scattering of CMB photons by the hot electrons of the ICM. The SZ effect was predicted by [Zeldovich & Sunyaev \(1969\)](#) and [Sunyaev & Zeldovich \(1972\)](#) and first detected by [Birkinshaw et al. \(1984\)](#). [Komatsu & Kitayama \(1999\)](#) provided the formalism for the accurate calculation of the SZ power spectrum and advocated its use in the cosmological context, as further developed by [Komatsu & Seljak \(2002\)](#).² These previous works developed the tools to use the SZ power spectrum to shed light on standard cosmological parameters, in particular σ_8 and Ω_m . The potential for SZ observables to probe extended cosmologies, e.g., related to primordial non-Gaussianity, massive neutrinos and dark energy, was emphasised by, e.g., [Weinberg et al. \(2013\)](#); [Hill & Pajer \(2013\)](#); [Roncarelli et al. \(2015\)](#); [Planck Collaboration \(2016c\)](#); [McCarthy et al. \(2018\)](#); [Salvati et al. \(2018\)](#); [Bolliet et al. \(2018\)](#); [Simons Collaboration \(2018\)](#); [Bocquet et al. \(2018\)](#). In addition, the evolution of the number of clusters, i.e., ‘cluster counts’, with redshift has long been known to provide a sensitive probe of cosmology (e.g., [Kaiser 1986, 1991](#); [Peebles et al. 1989](#); [Barbosa et al. 1996](#); [Holder et al. 2001](#); [Battye & Weller 2003](#)). Here we follow [Costanzi et al. \(2013\)](#) for the calculation of the halo mass function (HMF) when neutrinos are massive, and extend the framework developed for `class_sz` ([Bolliet et al. 2018](#)) to consistently include massive neutrinos in the theoretical models for the the SZ power spectrum and cluster counts.

¹ For reviews on neutrino cosmology, see, e.g., [Lesgourgues & Pastor \(2006\)](#); [Hannestad \(2010\)](#); [Lesgourgues et al. \(2013\)](#); [Abazajian et al. \(2016\)](#); [Lattanzi & Gerbino \(2018\)](#) or more foundational papers such as [Hu et al. \(1998\)](#); [Bashinsky & Seljak \(2004\)](#).

² For reviews on SZ science, see, e.g., [Carlstrom et al. \(2002\)](#) and [Mroczkowski et al. \(2019\)](#), where the latter highlights the potential of future high-resolution SZ observations.

Recent experiments have produced large catalogues of cluster SZ observations, in particular Atacama Cosmology Telescope (ACT, [Hasselfield et al. 2013](#)), South Pole Telescope (SPT, [Bleem et al. 2015](#)) and the Planck satellite ([Planck Collaboration 2016d](#)). Moreover, the Planck Collaboration obtained the first all-sky Compton- y map and its associated SZ power spectrum ([Planck Collaboration 2013b](#)). From these data sets, a number of works have performed cosmological parameter extraction analyses (e.g., [Planck Collaboration 2015, 2016c](#); [Hurier & Lacasa 2017](#); [Salvati et al. 2018](#); [Bolliet et al. 2018](#); [Bocquet et al. 2018](#); [Hill et al. 2014](#)). Most of these analyses have obtained a best-fit cosmology with a best-fit matter clustering amplitude σ_8 noticeably lower than the one from Planck 2015 primary CMB data (by $\approx 1 - 2\sigma$). This motivated a stream of research that attempted to identify the origin of the mismatch (e.g., [Dolag et al. 2016](#); [Bocquet et al. 2016](#); [Horowitz & Seljak 2017](#); [Bolliet et al. 2018](#); [Makiya et al. 2018](#); [Remazeilles et al. 2019](#); [Salvati et al. 2019](#); [Ruppin et al. 2019](#)). In particular, for analyses based on the X-ray calibrated $Y_{\text{SZ}}-M$ scaling relations (see, e.g., [Nagai 2006](#)), a significant attention has been brought to the hydrostatic mass bias, a parameter that quantifies the cluster mass fraction that is missed by X-ray measurements due to the underlying use of the hydrostatic equilibrium (HSE) assumption.

Our motivations in this paper are: to consistently include and study the effects of massive neutrinos on the SZ power spectrum and cluster counts (Section 2-4); to update the constraints on matter clustering, X-ray mass bias and total neutrino mass coming from the Planck SZ data and compare with other cluster and galaxy survey constraints (Section 5.1-5.5); to discuss whether massive neutrinos or dark energy can help explaining why the X-ray mass bias extracted from the combination of Planck SZ plus Planck primary CMB is in tension with the HSE expectation (Section 5.6-5.8); to assess the constraining power of future SZ power spectrum measurements (Section 6).

In Section 2 we present the calculation of the HMF and the SZ power spectrum for cosmological models with massive neutrinos. We then discuss the importance of the ‘cb’ prescription for the HMF in Section 3. Section 4 reviews the effects of massive neutrinos on the SZ power spectrum and cluster counts, while in Section 5 we present our constraints on the total neutrino mass based on the Planck SZ data. In Section 6 we present forecasts for cosmic variance limited SZ power spectrum experiments. We discuss our results and conclude in Section 7.

Definitions and general settings

We study three degenerate active neutrinos³, with a total neutrino mass Σm_ν , in spatially flat ΛCDM or $w\text{CDM}$ cosmologies with constant dark energy equation of state w . We keep the effective number of neutrino species fixed to the nominal value $N_{\text{eff}} = 3.046$ (e.g., [Mangano et al. 2005](#); [de Salas & Pastor 2016](#)).

³ The degenerate scenario is a better approximation to the realistic normal hierarchy and inverted hierarchy scenarios than models with one massive plus two massless or one massless plus two massive species ([Lesgourgues & Pastor 2006](#)).

We use the notations n_s and A_s for the spectral index and the amplitude of the primordial power spectrum of curvature perturbation; ρ_{crit} for the critical density of the universe today; $\Omega_c, \Omega_b, \Omega_\gamma, \Omega_\nu$ for the present CDM, baryons, photons and neutrino density fractions respectively; $\Omega_m = \Omega_c + \Omega_b + \Omega_\nu + \Omega_\gamma$ for the present matter density fraction; τ for the reionization optical depth; H_0 and $h = H_0/(100 \text{ km/s/Mpc})$ for the Hubble constant and reduced Hubble constant; θ_s for the angular size of the sound horizon at decoupling; $f_\nu \equiv \Omega_\nu/\Omega_m$ for the neutrino fraction; $\omega_x = \Omega_x h^2$ for the physical densities of species $x = c, b, \nu, m$; σ_8 for the variance of the matter over-density field smoothed by a sphere of radius $8 \text{ Mpc}/h$.

For our numerical calculations, unless otherwise stated, we use a fiducial (or reference) ΛCDM cosmology with parameters: $h = 0.7$, $\Omega_b = 0.05$, $\Omega_c = 0.26$, $\tau = 0.07$, $A_s = 1.93 \times 10^{-9}$, $n_s = 0.96$ and $\Sigma m_\nu = 0.06 \text{ eV}$. This model has $\sigma_8 = 0.80$ and $100\theta_s = 1.0510$. For the modelling of the SZ power spectrum and cluster counts, we use the Tinker et al. (2008) HMF interpolated at M_{500c} , the Planck Collaboration (2013a) pressure profile (see Bolliet et al. 2018, for details), and, when not varied or unless otherwise stated, a reference X-ray mass bias $B = 1.41$ corresponding to $(1-b) = 1/B \simeq 0.7$. We denote as $B_{\text{HSE}} = 1.25$ and $b_{\text{HSE}} = 0.2$ the values associated with the hydrostatical equilibrium assumption for the ICM (e.g., Kay et al. 2004; Nagai et al. 2007a; Shi et al. 2016).

2 SZ POWER SPECTRUM AND CLUSTER COUNTS WITH MASSIVE NEUTRINOS

Here we recall the theoretical framework for the computations of the SZ power spectrum (Section 2.1) and SZ cluster counts (Section 2.2) with massive neutrinos. Then, in Section 2.3 we briefly review the role the X-ray mass bias parameter in the Planck SZ analyses.

2.1 Power spectrum

We compute the SZ power spectrum according to the halo model of structure formation (see Cooray & Sheth (2002) for a review of the halo model, and Komatsu & Kitayama (1999) for its application to the SZ power spectrum). Here, we only consider the 1-halo contribution to the SZ power spectrum, as the 2-halo term is at least one order of magnitude smaller on scales of observational interest (e.g., Komatsu & Kitayama 1999; Hill & Pajer 2013; Horowitz & Seljak 2017). The model of the SZ power spectrum has three main ingredients: the differential volume element, $dV/(dzd\Omega)$ with respect to redshift and solid angle, the HMF, $dN/dM dV$, and the square of the 2d Fourier transform of the ICM electron pressure profile integrated over the line-of-sight, $|y_\ell(M, z)|^2$. The angular power spectrum of the SZ effect is obtained by integrating the product of these three quantities over redshift, z , and cluster masses, M :

$$C_\ell^{\text{SZ}} = \int dz \int dM \frac{dV}{dzd\Omega} \frac{dN}{dM dV} |y_\ell(M, z)|^2. \quad (1)$$

With massive neutrinos, the differential volume element and Fourier transform of the pressure profile can be computed without modifications (see, e.g., Bolliet et al. 2018). However,

the calculation of the HMF needs some revision. Costanzi et al. (2013) performed N-body simulations incorporating massive neutrinos. In agreement with Ichiki & Takada (2012) and subsequent work of LoVerde (2014), they showed that the Tinker et al. (2008) fitting formula remains valid for the HMF, provided one does not use the total linear matter power spectrum and the total matter density but rather the power spectrum of CDM and baryons, $P_{\text{cb}}(k, z)$, and the density $\rho_{\text{cb}} = (\Omega_c + \Omega_b)\rho_{\text{crit}}$ in the calculation of the variance of the smoothed over-density field $\sigma(M, z)$. More explicitly, the square of this quantity is given by

$$\sigma^2(M, z) = \int \frac{dk}{k} \frac{k^3}{2\pi^2} P_{\text{cb}}(k, z) W^2(kR), \quad (2)$$

where $R = [3M/4\pi\rho_{\text{cb}}]$ and $W(x)$ is the top-hat window function. This ‘cb’ prescription is consistent with the physical expectation that neutrinos do not cluster as much as baryons and CDM, and thus, do not trigger the formation of compact objects (see, e.g., LoVerde 2014, for details).

2.2 Cluster counts

SZ cluster surveys are sensitive to the cluster signal-to-noise. For a cluster of mass M at redshift z , the predicted signal-to-noise is computed using the $Y_{\text{SZ}} - M$ and $\theta - M$ relation, where Y_{SZ} is the SZ flux and θ the angular size associated with the cluster. We use the same relations as Planck Collaboration (2016c), where the spherical over-density mass defined with respect to $500\rho_{\text{crit}}$, say $M_{500c}^{\text{X-ray}}$, is a biased estimator of the true halo mass M_{500c}^{true} , i.e., $M_{500c}^{\text{X-ray}} = M_{500c}^{\text{true}}/B$, with B the X-ray mass bias discussed in the next subsection. Once θ and Y_{SZ} are known for a given mass, we compute the signal-to-noise as $\xi = Y_{\text{SZ}}(M, z)/\sigma(\theta; l, b)$ where σ is obtained by interpolating the experiment’s noise map at galactic coordinate⁴ (l, b) and angular size θ . The theoretical number of clusters in each signal-to-noise bin centred on ξ_j and redshift bin centred on z_i is then given by $\bar{N}_{ij} = (dN/dz d\xi) \Delta z_i \Delta \xi_j$, with

$$\frac{dN}{dz d\xi} = \int d\Omega \int dM \frac{dV}{dz d\Omega} \frac{dN}{dM dV} \mathcal{P}(\xi, \xi_j). \quad (3)$$

Here \mathcal{P} is the detection probability for clusters in the signal-to-noise bin ξ_j . For the detection probability we use an analytical approximation with the ‘erf’ completeness (see Eq. 14 in Planck Collaboration 2016c), and a detection threshold that we keep fixed to $\xi_{\text{cut}} = 6$, as was done in the baseline Planck Collaboration (2016c) analysis.

2.3 Role of the X-ray mass bias parameter

A mass bias parameter is present in the Planck SZ analyses because the scaling relations between the SZ flux and size of clusters on one hand, and the cluster masses, on the other hand, are calibrated on X-ray measurements that use hydrostatic mass estimates (see Appendix A of Planck Collaboration 2014b). The ‘true’ mass of a cluster is not a direct observable. It can only be inferred from the measurements of other observables, that constitute *mass proxies*, complemented by assumptions for the hydrodynamical state and

⁴ Here b is a galactic coordinate and has nothing to do with the X-ray mass bias also dubbed b in the next Section.

geometry of the cluster. Kravtsov et al. (2006) discussed several mass proxies, for instance the X-ray temperature T_X , X-ray luminosity L_X , the integrated SZ flux of the ICM Y_{SZ} (e.g., Nagai 2006), or the low-scatter $Y_X \equiv M_{\text{gas}} T_X$ introduced by Kravtsov et al. (2006). One then relies on models and assumptions to compute the cluster mass from X-ray observations. For instance, the masses of the Chandra sample of Vikhlinin et al. (2006) are estimated using models for the gas density and temperature profiles (calibrated on X-ray observations) as well as the assumption of hydrostatic equilibrium (HSE) and spherical symmetry (e.g., Sarazin 1986). Then it is possible to construct the relation between the mass proxy, Y_X or Y_{SZ} , and the X-ray mass estimate, or eventually the spherical over-density mass $M_{500c}^{X\text{-ray}}$, by fitting the observational data.⁵

The true mass is generally larger than the HSE mass. Numerical simulations suggest that the HSE mass is biased low by $b \approx 20\%$ with respect to the true mass, corresponding to $B_{\text{HSE}} = 1.25$ (e.g., Kay et al. 2004; Nagai et al. 2007a; Lau et al. 2009; Battaglia et al. 2012; Nelson et al. 2014). Such bias arises due to non-thermal pressure and recent analytical work have been successful in modelling it fairly (e.g., Shi & Komatsu 2014; Shi et al. 2015, 2016). Although numerical work relying on the ART code (Kravtsov et al. 2002) find a HSE bias that is mass independent, the recent BAHAMAS and MACSIS simulations are suggesting a mass dependent HSE bias that reaches $\approx 40\%$ for heavy clusters with $M_{500c} \gtrsim 10^{15} M_\odot$ (Henson et al. 2017). In this paper we do not study mass-dependent bias, however, we note that a larger bias for heavier clusters would have the effect of boosting the SZ power at large scales where heavier clusters contribute more (e.g., Figure 1 of Remazeilles et al. 2019). This could drive the value of σ_8 extracted from the SZ power spectrum analysis to a larger value, more consistent with Planck primary CMB.

In fact, the X-ray mass bias can be used as a phenomenological parameterisation of departure from other assumptions than HSE, and of systematics and physical processes that are yet to be better understood (e.g., Pratt et al. 2019). Here, we either use the mass bias as a free parameter, or set a Gaussian prior around the HSE value, typically expected to be $(1 - b) \simeq 0.8$ from numerical simulations (e.g., Kay et al. 2004; Nagai et al. 2007a; Shi et al. 2016). Several observational constraints on the X-ray mass bias are shown on the right panel of Figure 5, along with the results we obtain in Section 5. The relative precision on the X-ray mass bias is currently at the $\sim 10\%$ level and is expected to reach the 1% level in the next decade (e.g., Louis & Alonso 2017).

3 IMPORTANCE OF THE ‘CB’ PRESCRIPTION

For the numerical computations of the SZ power spectrum and SZ cluster counts, we use `class_ssz`⁶ (Bolliet et al. 2018), a publicly available extension of the `class` code (Blas et al.

2011). We updated `class_ssz` to take into account the ‘cb’ prescription. Since Ichiki & Takada (2012), Costanzi et al. (2013) and LoVerde (2014) have already studied the effect of the ‘cb’ prescription on the cluster counts, we focus here on the SZ power spectrum. Figure 1 shows the relative difference for the SZ power spectrum that arises when the ‘cb’ prescription is used, for several values of Σm_ν . This difference can be understood as follows: the current fraction of non-relativistic matter density in the form of neutrinos, $f_\nu = \omega_\nu / \omega_m$, is given by $f_\nu \simeq \Sigma m_\nu / 14 \text{ eV}$ with our fiducial parameter values. The total matter power spectrum is given by a weighted sum over the ‘cb’ power spectrum, the neutrino one and the cross-correlation term: $P_m = (1 - f_\nu)^2 P_{cb} + f_\nu^2 P_\nu + 2f_\nu(1 - f_\nu) P_{cb \times \nu}$. On scales smaller than the neutrino free-streaming scale, neutrino density perturbations are much smaller than baryon and CDM perturbations, such that $P_m \simeq (1 - f_\nu)^2 P_{cb}$. Since this is true in particular for the scale $R = 8 h^{-1} \text{ Mpc}$, the relation between the corresponding values of σ_8 is

$$\sigma_8^m \simeq (1 - f_\nu) \sigma_8^{cb}, \quad (4)$$

where we used superscript ‘m’ and ‘cb’ to indicate whether σ_8 is computed with P_m or P_{cb} . Next, we recall that the SZ power spectrum scales as $(\sigma_8^m)^{8.1} \Omega_m^{3.2}$ (for $\ell < 10^3$) without massive neutrinos. According to the ‘cb’ prescription, it now scales as $(\sigma_8^{cb})^{8.1} \Omega_{cb}^{3.2}$ in presence of massive neutrinos. Using Eq. (4) and $\Omega_{cb} = (1 - f_\nu) \Omega_m$, we deduce that the relative difference between both should be given by $\Delta C_\ell^{\text{SZ}} / C_\ell^{\text{SZ}} \approx 4.9 f_\nu$, with a larger power spectrum for the ‘cb’ prescription. With our fiducial model this corresponds to $\Delta C_\ell^{\text{SZ}} / C_\ell^{\text{SZ}} \approx \Sigma m_\nu / (2.9 \text{ eV})$. This is a very good approximation to the ratios observed in Figure 1 on small angular scales (high multipoles) where neutrino perturbations are negligible compared to baryon and CDM perturbations. On large angular scales (low multipoles), P_m also picks up some contributions from neutrino perturbations. Thus the difference between the SZ spectrum computed with or without the ‘cb’ prescription is smaller at low multipole.

With this we conclude that an SZ power spectrum analysis without the ‘cb’ prescription would yield a constraint on σ_8 biased high by $\approx 0.25\%$ if the total neutrino mass was fixed to $\Sigma m_\nu = 0.06 \text{ eV}$. Thus the ‘cb’ prescription does not appear to be crucial for small neutrino masses, in line with expectations. Note, however, that the total neutrino mass is not strongly constrained by SZ clusters and power spectrum when they are not combined with other data sets. Hence, the maximum likelihood analysis can sample relatively large neutrino masses for which the ‘cb’ prescription becomes important. For instance, our analysis of the Planck SZ cluster counts alone has a best-fitting value at $\Sigma m_\nu = 4.35 \text{ eV}$. For such a large neutrino mass, the predicted number of clusters differs by about 25% with or without the ‘cb’ prescription. Then, for consistency, it is important to take it into account.

4 EFFECT OF MASSIVE NEUTRINOS ON SZ OBSERVABLES

The matter power spectrum is damped by massive neutrino free-streaming (e.g., Eisenstein & Hu 1997; Hu & Eisenstein 1998; Lesgourgues & Pastor 2006). The free-streaming scale is inversely proportional to the total neutrino mass and reaches a maximum at radiation-to-matter equality.

⁵ Since the mass estimate that enters the constructed $Y_X - M_{500c}^{X\text{-ray}}$ or $Y_{SZ} - M_{500c}^{X\text{-ray}}$ relations relies on HSE, it is some times called the hydrostatic mass.

⁶ website: https://github.com/borisbolliet/class_ssz_public

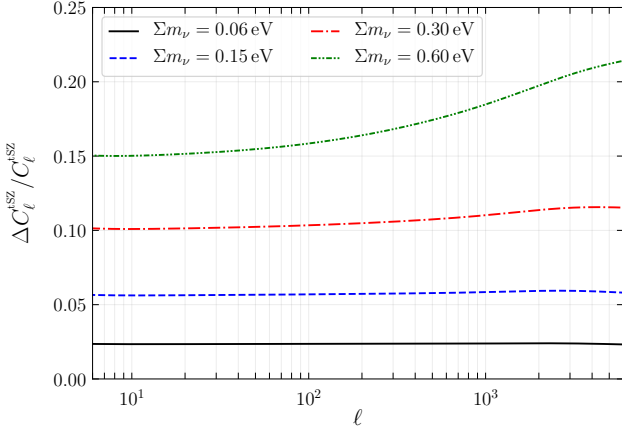


Figure 1. Relative difference between SZ power spectrum computed with and without the ‘cb’ prescription. We use the notation $\Delta Q/Q \equiv (Q^{\text{cb}} - Q)/Q$ where the superscript ‘cb’ indicates the correct modelling. For instance, at $\Sigma m_\nu = 0.30$ eV, omitting the ‘cb’ prescription leads to an under-estimation of the SZ power spectrum amplitude by about 10%. Here, Σm_ν is varied while $(A_s, n_s, \omega_c, \omega_b, \theta_s)$ are set to their fiducial values: this choice is ‘case B’ in section 4.

Wavelengths larger than the maximum free-streaming scale are not affected by the damping, while wavelengths smaller than the current free-streaming scale are maximally affected. This being said, the global impact of massive neutrinos on cosmological observables is subtle to describe, because a variation of Σm_ν induces variations of other parameters. These variations and their observable effects depend on which quantities one chooses to keep fixed while varying Σm_ν (or $\omega_\nu \simeq \Sigma m_\nu/93.14$ eV). We pick three examples:

Case A: We keep the quantities $(A_s, n_s, \omega_b, \Omega_m, h)$ fixed (and therefore, also Ω_Λ and ω_m), while adjusting the CDM density to $\omega_c = \omega_m - \omega_b - \omega_\nu$. This choice is the most conventional one when discussing the effect of neutrino free-streaming on the matter power spectrum. Indeed, it fixes the amplitude of the large-scale power spectrum, and singles out the small-scale step-like suppression induced by massive neutrinos. Note, however, that the redshift of radiation-to-matter equality is not constant in that case. Indeed, for realistic neutrino masses, neutrinos still count as radiation at equality, and $z_{\text{eq}} = (\omega_b + \omega_c)/\omega_r$, where ω_r accounts for the density of photons plus relativistic neutrinos. In this case, when Σm_ν increases, ω_c decreases, and so does z_{eq} . It is with this choice that the linear total matter power spectrum is suppressed roughly by $(1 - 8f_\nu)$ in the small-scale limit (Eisenstein & Hu 1997; Lesgourgues & Pastor 2006), while the linear ‘cb’ power spectrum is suppressed by $(1 - 6f_\nu)$ as explained in Vagnozzi et al. (2018). Moreover, the actual suppression is not perfectly linear in f_ν and also depends on the mass splitting. Finally, the quantity $(\sigma_8)^2$, which is of particular interest for the rest of the discussion, is sensitive to scales on which the neutrino free-streaming effect is not maximal. Using `class`, we find that for $f_\nu = \mathcal{O}(10^{-2})$ and three degenerate massive neutrinos,

$$(\sigma_8^{\text{m}})^2 \propto (1 - 7.3f_\nu) \quad \text{while} \quad (\sigma_8^{\text{cb}})^2 \propto (1 - 5.5f_\nu).$$

Meanwhile the fractional density of baryons and CDM scales simply like $\Omega_{\text{cb}} \propto (1 - f_\nu)$.

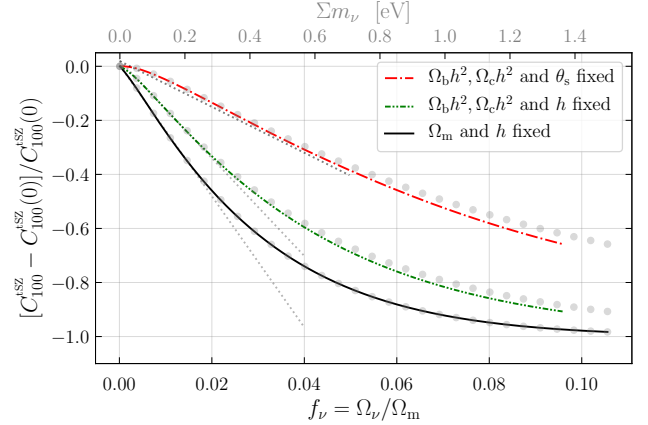


Figure 2. Relative variation of the SZ power spectrum amplitude computed at multipole $\ell = 100$ with respect to the neutrino fraction f_ν , for different choices of parameterisation referred in the text as case B, C, A (from top to bottom). The grey dotted lines are the tangent near the origin with slope $\approx -8, -18$, and -25 .

Case B: We fix the quantities that are best measured by CMB experiments, i.e., the redshift of equality z_{eq} (and thus ω_c) and the angular scale of the sound horizon at decoupling θ_s . Concretely, one can fix $(A_s, n_s, \omega_b, \omega_c, \theta_s)$, and increase Σm_ν while decreasing h in such a way to keep a fixed θ_s .

Here, the matter clustering amplitude is suppressed as $(\sigma_8^{\text{m}})^2 \propto (1 - 6.6f_\nu)$ and $(\sigma_8^{\text{cb}})^2 \propto (1 - 4.9f_\nu)$,

again for $f_\nu = \mathcal{O}(10^{-2})$ and degenerate masses. In this case, maintaining a fixed θ_s requires that h varies with the total neutrino mass according to $\Delta h \simeq -0.083\Delta(\Sigma m_\nu/1 \text{ eV})$, a result consistent with Eq. (2.1) of Archidiacono et al. (2017). For our fiducial parameter values this is equivalent to $h \propto (1 - 1.6f_\nu)$.

Case C: For illustrative purposes, we mention a third possible choice. One may fix $(A_s, n_s, \omega_b, \omega_c, h)$ and increase Σm_ν : this transformation maintains a fixed redshift of equality, but not a fixed angular scale θ_s . In this case, the linear matter power spectrum is suppressed by different factors on large and small scales, while $(\sigma_8^{\text{m}})^2 \propto (1 - 5.9f_\nu)$ and $(\sigma_8^{\text{cb}})^2 \propto (1 - 4.1f_\nu)$.

It is then possible to estimate analytically the impact of the total neutrino mass on the SZ power spectrum in each of these cases, and to compare these estimates with the numerical results shown in Figure 2. The SZ power spectrum scales like

$$C_\ell^{\text{tSZ}} \propto (\sigma_8^{\text{m}})^{8.1} (\Omega_m)^{3.2} B^{-3.2} h^{-1.7} \quad \text{for } \ell \lesssim 10^3 \quad (5)$$

in absence of massive neutrinos (e.g., Komatsu & Seljak 2002; George et al. 2015; Bolliet et al. 2018). So, with the ‘cb’ prescription we now expect

$$C_\ell^{\text{tSZ}} \propto (\sigma_8^{\text{cb}})^{8.1} (\Omega_{\text{cb}})^{3.2} B^{-3.2} h^{-1.7} \quad \text{for } \ell \lesssim 10^3 \quad (6)$$

in presence of massive neutrinos.

This scaling and the above discussion leads to $C_\ell^{\text{tSZ}} \propto (1 - \lambda f_\nu)$ with $\lambda \approx -25, -7$ and -17 in case A, B and C respectively in good agreement with the slopes of Figure 2. This confirms that the extrapolation of Eq. (6) to models with three degenerate massive neutrinos is valid.

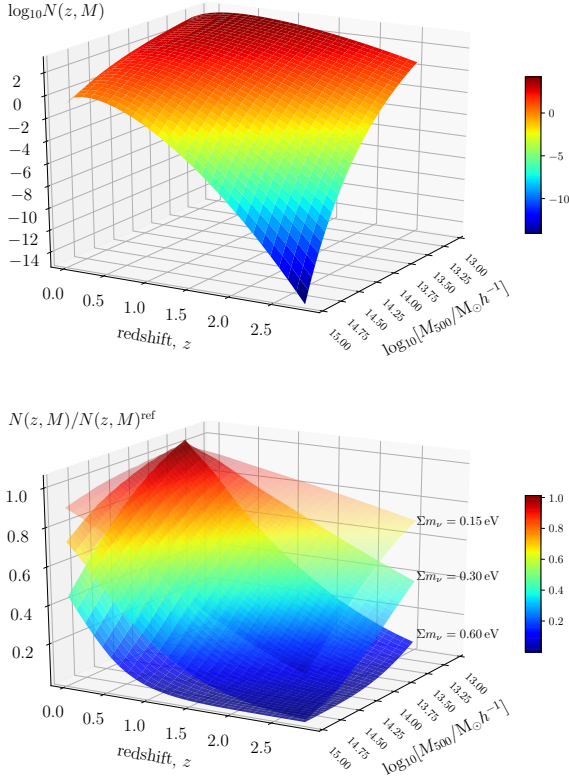


Figure 3. (Top panel) Cluster counts $N(z, M)$ for $\Sigma m_\nu = 0.06$ eV. (Bottom panel) Variation of $N(z, M)$ with respect to the total neutrino masses. We plot the ratio of $N(z, M)$ computed with three different neutrino masses over the previous one, with the choice of parametrization called ‘case B’ in the text (i.e., fixed A_s , n_s , ω_b , ω_c , and θ_s).

The fact that the scaling of the amplitude of the SZ power spectrum with the total neutrino mass depends on the chosen parameter basis also applies to cluster counts. We show the effect of the total neutrino mass on $N(z, M)$ for ‘case B’ in figure 3. The suppression of cluster abundance is larger at large cluster masses and high redshift because this regime is determined by the exponential tail of the HMF (e.g., Lukic et al. 2007).

Although they are not used in the paper, for completeness we give the scaling of the total cluster counts for fixed neutrino masses. At fixed total neutrino mass, the scaling of cluster counts with cosmological parameters depends on the survey completeness (as well as the mass and redshift ranges). We find that the number of clusters scales as

$$N_{\text{tot}} \propto \sigma_8^{9.8} \Omega_m^{2.9} B^{-3.2} h^{-0.5}$$

where N_{tot} is the sum of the clusters in all the redshift and signal-to-noise bins of the Planck analysis. Without the survey completeness the scaling becomes $N_{\text{tot}} \propto \sigma_8^{4.3} \Omega_m^{1.5} h^{0.5}$. Note that here and hereafter σ_8 means σ_8^m .

5 CURRENT CONSTRAINTS

We study the constraints that can be derived from the Planck SZ data on the Λ CDM model with a fixed $\Sigma m_\nu = 0.06$ eV (Sections 5.3–5.5), on the $\nu\Lambda$ CDM model with a varying total

neutrino mass (Sections 5.6–5.7), and finally on the νw CDM model when additionally varying the dark energy equation of state parameter w (Section 5.8). We sample the parameter space with Monte Carlo Markov Chains (MCMCs) using MontePython⁷ (Brinckmann & Lesgourgues 2018; Audren et al. 2013a). For the computation of the SZ power spectrum, cluster counts, and CMB spectra we use `class_ssz` (Bolliet et al. 2018) including the changes described above, i.e., the ‘cb’ prescription (see Section 3).

5.1 Parameter combinations

The scaling of the SZ power spectrum given in Eq. (6) motivates the definition of the parameter

$$F_{\text{cb}} \equiv \sigma_8^{\text{cb}} (\Omega_{\text{cb}}/B)^{0.4} h^{-0.2} \quad (7)$$

for the characterisation of the SZ power spectrum amplitude, analogous to the parameter

$$F \equiv \sigma_8 (\Omega_m/B)^{0.4} h^{-0.2} \quad (8)$$

used in Bolliet et al. (2018). In the MCMC analysis of the Planck y -map power spectrum data, this is the parameter combination that minimises the relative uncertainty: if we write $F = \sigma_8^{\text{cb}} (\Omega_{\text{cb}}/B)^\lambda h^\gamma$, we find that $\sigma(F)/F$ is minimal for $\lambda = 0.4$ and $\gamma = -0.2$. For the Planck SZ cluster counts analysis, we find that the ‘best’ parameter combinations with respect to this criterion are

$$F_{\text{cb}}^* \equiv \sigma_8^{\text{cb}} (\Omega_{\text{cb}}/B)^{0.35}, \quad (9)$$

$$F^* \equiv \sigma_8 (\Omega_m/B)^{0.35}, \quad (10)$$

where we note that the Hubble parameter does not appear. This is consistent with White et al. (1993) who found on the basis of the Press-Schechter formula that the cluster counts probe mainly the combination $\sigma_8 \Omega_m^{0.32}$. When the X-ray mass bias B is fixed or constrained, we also use the parameter combinations

$$S_8^{0.2} \equiv \sigma_8 (\Omega_m/0.3)^{0.2} \quad (11)$$

for the Planck SZ cluster counts analyses (as was used in Bocquet et al. 2018, for the SPT-SZ analysis) and

$$S_8^{0.4} h_{70}^{-0.2} \equiv \sigma_8 (\Omega_m/0.3)^{0.4} h_{70}^{-0.2} \quad (12)$$

for the Planck y -map power spectrum analyses. We also discuss constraints on $S_8 \equiv \sigma_8 (\Omega_m/0.3)^{0.5}$ commonly used in large-scale structure analyses.

5.2 Data and likelihoods

We use the Planck 2015 y -map power spectrum (Planck Collaboration 2015) and Planck 2015 cosmological sample of the SZ cluster catalogue (Planck Collaboration 2016c). To avoid complications related to the covariance between cluster counts and SZ power spectrum, we do not study joint constraints from the Planck y -map power spectrum and Planck SZ cluster counts, but only use them separately. We use uniform priors on input parameters reported in Table 1.

⁷ The new MontePython version 3.1 is available at https://github.com/brinckmann/montepython_public.

Parameter	Min.	Max.
$10^9 A_s$	1.8	2.7
n_s	0.8	1
τ	0.04	0.12
h	0.50	>0.85
$\Omega_b h^2$	0.0199	0.0245
$\Omega_c h^2$	0.09	—
w	−3	−0.5
Σm_ν [eV]	0	—
B	1	—
A_{CIB}	0	10
A_{IR}	0	10
a_{RS}	−10	10
$\log_{10} Y_\star$	−0.3	−0.08
σ_Y	0.02	0.12
α	1	3

Table 1. Uniform priors used in the maximum likelihood analysis. The notation ‘—’ means no bound. The nuisance parameter a_{RS} is related to A_{RS} of Bolliet et al. (2018) via $A_{\text{RS}} = \exp(-a_{\text{RS}})$.

	mean \pm σ
$\log_{10} Y_\star$	-0.19 ± 0.02
σ_Y	0.075 ± 0.01
α	1.79 ± 0.08

Table 2. Gaussian priors on the cluster counts likelihood parameters, the same as in Planck Collaboration (2016c).

For the Planck y -map power spectrum likelihood we follow Bolliet et al. (2018). We fit the Planck 2015 y -map power spectrum in eighteen multipole bins between $\ell_{\text{min}} = 10$ and $\ell_{\text{max}} = 959.5$, including non-Gaussian errors. We sample the three foreground residual amplitudes⁸ (A_{CIB} , A_{IR} , a_{RS}) in addition to the cosmological parameters and X-ray mass bias.

For the Planck SZ cluster counts likelihood, we use the same model and likelihood as the Planck Collaboration (2016c) baseline analysis, i.e., with fixed $\beta = 0.66$ and the Gaussian priors on the scaling relations parameters α , $\log_{10} Y_\star$ and σ_Y reported in Table 2 as well as a detection threshold $\xi_{\text{cut}} = 6$, using information on both signal-to-noise and redshift dimensions. We ported the CosmoMC (Lewis & Bridle 2002) likelihood code `szcounts.f90` into `class_sz` and MontePython. We refer to Planck Collaboration (2016c) and Zubeldia & Challinor (2019) for a detailed description of the cluster counts likelihood and definitions of α , Y_\star , β , σ_Y .

We also study combinations of the Planck SZ probes with the following datasets:

- **Planck 2015 primary CMB** consisting of Planck 2015 high- ℓ temperature and polarisation (TT,TE,EE) plus low- ℓ temperature (Planck Collaboration 2016a) and a Gaussian prior on the reionisation optical depth⁹ intended to mimic the constraint from the Planck 2016 low- ℓ polarisation

likelihood (‘SimLow’, Planck Collaboration 2016e) as in Calabrese et al. (2017b), i.e. $\tau = 0.06 \pm 0.01$.¹⁰

- **BAO** consisting of data from the 6dFGS (Beutler et al. 2011), the SDSS DR7 MGS (Ross et al. 2015) and the BOSS DR12 LOWZ & CMASS galaxy samples (Alam et al. 2017).

The Planck high- ℓ TT,TE,EE likelihood has three ‘nuisance’ parameters related to the SZ effect (Planck Collaboration 2014a, 2016a): $\xi^{\text{tSZ} \times \text{CIB}}$ to account for the correlation between SZ and CIB foregrounds; A^{kSZ} for the amplitude of the kinetic SZ power spectrum; and A^{tSZ} for the amplitude of the thermal SZ power spectrum template. The template for the thermal SZ power spectrum used in the Planck CMB likelihood is the model of Efstathiou & Migliaccio (2012) (with pressure profile evolution parameter $\epsilon = 0.5$). Motivated by a SPT measurement (Reichardt et al. 2012), the Planck CMB likelihood has a conservative Gaussian prior on the linear combination

$$A^{\text{kSZ}} + 1.6A^{\text{tSZ}} = (9.5 \pm 3)\mu\text{K}^2 \quad (13)$$

(Planck Collaboration 2016b) as well as a uniform prior on $\xi^{\text{tSZ} \times \text{CIB}}$ between 0 and 1 (justified by the SPT constraint of George et al. 2015). In this work, we use the same settings for the SZ templates and nuisance parameters as in the Planck CMB likelihood.¹¹

5.3 Planck y -map power spectrum alone

In ΛCDM with $\Sigma m_\nu = 0.06$ eV, we measure F to a $\approx 3\%$ precision:

$$F = 0.455 \pm 0.013 \text{ (68\% CL)}.$$

Without the ‘cb’ prescription, we find $F = 0.456 \pm 0.013$ (68% CL), i.e., a negligible $\approx 0.2\%$ upward shift, as anticipated in Section 3. We note that our constraint on F in ΛCDM , without the ‘cb’ prescription, is 1% lower than the one quoted Bolliet et al. (2018). This small difference is due to the new version of `class_sz` which uses an original `class` routine for the computation of $\sigma(R)$ instead of the method based on Chebyshev polynomial interpolation of the previous version.

In $\nu\Lambda\text{CDM}$, the total neutrino mass is not constrained by the Planck y -map power spectrum data alone. In our analysis, the 95% CL interval for Σm_ν is determined by the upper bound of the H_0 prior. At large total neutrino mass there is an anti-correlation between Σm_ν and F_{cb} , so the $\nu\Lambda\text{CDM}$ constraint on F_{cb} is also prior driven. Nevertheless, for $\Sigma m_\nu < 0.1$ eV, the 68% and 95% CL intervals of F_{cb} are independent of Σm_ν with $F_{\text{cb}} = 0.456 \pm 0.013$ (68% CL).

¹⁰ This value agrees with the Planck 2018 results (Planck Collaboration 2018), $\tau = 0.054 \pm 0.08$ (68% CL).

¹¹ Although, as emphasised in Planck Collaboration (2016b), the Gaussian prior of Eq. (13) and the uniform prior on $\xi^{\text{tSZ} \times \text{CIB}}$ are sufficient to eliminate the sensitivity of the cosmological parameters on the SZ modelling, we note that since the Planck y -map power spectrum constrains A^{tSZ} , the Gaussian prior of Eq. (13) could be further augmented with a Planck y -map motivated prior on A^{tSZ} .

⁸ ‘CIB’ refers to the cosmic infrared background, ‘RS’ and ‘IR’ to radio and infra-red point sources.

⁹ We never include a low- ℓ polarisation likelihood directly and we do not use Planck CMB lensing power spectra.

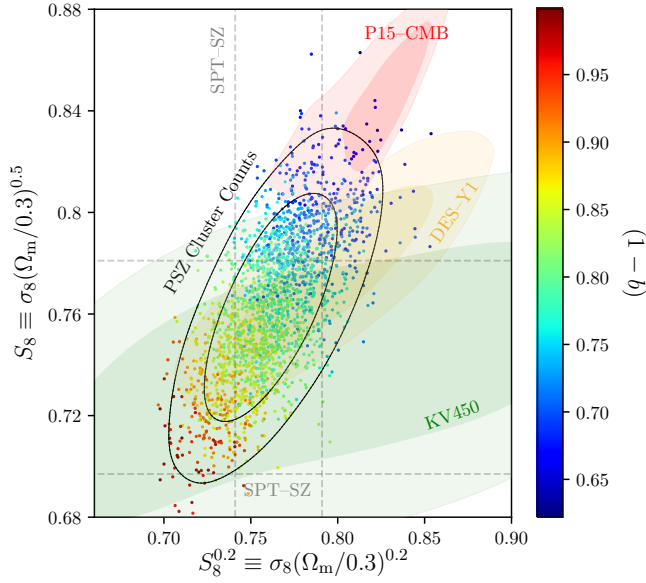


Figure 4. Marginalised 2d joint posterior probability distributions with 68% CL and 95% CL contours from the Planck cluster counts analysis with a Gaussian prior on the X-ray mass bias $B = 1.250 \pm 0.125$ (corresponding to $1 - b = 0.80 \pm 0.08$) in Λ CDM (black contours). The red Planck contours ‘P15-CMB’ are from our chains in $\nu\Lambda$ CDM. The orange ‘DES-Y1’ contours are from (DES Collaboration 2018) in $\nu\Lambda$ CDM ‘3x2pt’. The green contours ‘KV-450’ for KiDS+VIKING are from (Hildebrandt et al. 2018) in Λ CDM. The dashed lines show the $1-\sigma$ intervals from the SPT-SZ cluster counts analysis (‘SPTcl’, Bocquet et al. 2018).

5.4 Planck SZ cluster counts alone

In Λ CDM with $\Sigma m_\nu = 0.06$ eV, we measure F^* to a $\approx 1.5\%$ precision:

$$F^* = 0.460 \pm 0.007 \text{ (68\% CL)}.$$

If we do not adopt the ‘cb’ prescription, we obtain a value of F^* that is $\approx 0.2\%$ larger, as also found for the Planck y -map power spectrum analysis.

In $\nu\Lambda$ CDM, the total neutrino mass is unconstrained by the SZ cluster counts alone. Like in the Planck y -map power spectrum analysis, we find that the 95% CL interval for Σm_ν is determined by the upper bound of the H_0 prior. Thus, the $\nu\Lambda$ CDM constraint on F_{cb}^* is also prior driven. Nevertheless, for $\Sigma m_\nu < 0.1$ eV, the 68% and 95% CL intervals of F_{cb}^* are almost independent of Σm_ν with $F_{\text{cb}}^* = 0.461 \pm 0.007$ (68% CL).

5.5 Planck SZ with B_{HSE}

Motivated by the discussion of Section 2.3 we set a Gaussian prior on the X-ray mass bias centred on $B_{\text{HSE}} = 1/(1 - b_{\text{HSE}})$ with a 10% relative width, i.e., $B = 1.250 \pm 0.125$. With this prior, our analysis of Planck SZ cluster counts in Λ CDM with $\Sigma m_\nu = 0.06$ eV yields

$$\begin{aligned} S_8^{0.2} &= 0.763 \pm 0.025 \text{ (68\% CL)}, \\ S_8 &= 0.764 \pm 0.029 \text{ (68\% CL)}. \end{aligned}$$

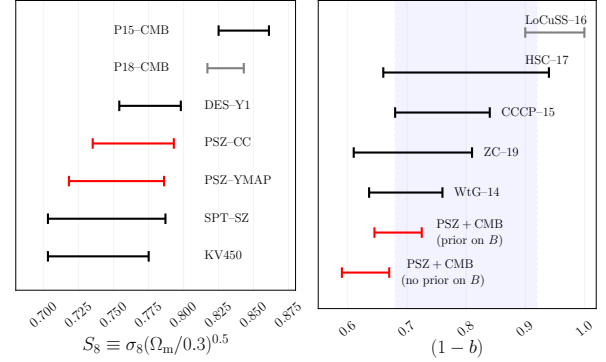


Figure 5. (Left panel) Marginalised $1-\sigma$ constraints on S_8 from several datasets. The grey constraints ‘P18-CMB’ refers to the latest Λ CDM measurement from (Planck Collaboration 2018). See caption of Figure 4 for the others. (Right panel) Marginalised $1-\sigma$ constraints on $(1 - b)$ from several datasets (see last paragraph of Section 5.7 for the references). The blue band is the simulation result of Shi et al. (2016) (see their Figure 5, ‘NG all’). Also reported are Weighing the Giants (WtG, von der Linden et al. 2014), Canadian Cluster Comparison Project (CCCP, Hoekstra et al. 2015), Subaru Hyper Suprime-Cam (HSC, Medezinski et al. 2017), Local Cluster Substructure Survey (LoCuSS, Smith et al. 2016), and the updated Planck CMB weak lensing constraint (ZC, Zubeldia & Challinor 2019). the ‘PSZ’ values are the median central values of the Planck SZ cluster counts and Planck SZ power spectrum analyses.

Our analysis of Planck y -map power spectrum in Λ CDM with $\Sigma m_\nu = 0.06$ eV yields

$$\begin{aligned} S_8^{0.4} h_{70}^{-0.2} &= 0.756 \pm 0.033 \text{ (68\% CL)}, \\ S_8 &= 0.752 \pm 0.034 \text{ (68\% CL)}. \end{aligned}$$

As illustrated on Figure 4 and on the left panel of Figure 5, the Planck SZ constraints are fully consistent with the results of SPT-SZ (Bocquet et al. 2018), DES-Y1 (DES Collaboration 2018) and KiDS+VIKING-450 (Hildebrandt et al. 2018), and in mild tension with Planck 2015 primary CMB (see Handley & Lemos 2019, for a discussion of the moderate tension between DES-Y1 and Planck). There are three straightforward ways to alleviate the small mismatch between Planck SZ and Planck 2015 primary CMB: a larger X-ray mass bias, more-massive neutrinos or a less-negative w . Our analyses presented hereafter suggest that the larger X-ray mass bias is preferred by the Planck data.

5.6 Planck SZ with Planck 2015 primary CMB

In $\nu\Lambda$ CDM, for Planck 2015 primary CMB alone we find $\Sigma m_\nu < 0.35$ eV (95% CL). When we do not use a prior constraint on the X-ray mass bias, the addition of Planck SZ improves the $2-\sigma$ limit slightly. For Planck 2015 primary CMB combined with Planck SZ cluster counts we obtain

$$\begin{aligned} F^* &= 0.464 \pm 0.006 \text{ (68\% CL)}, \\ (1 - b) &= 0.62^{+0.03}_{-0.04} \text{ (68\% CL)}, \\ \Sigma m_\nu &< 0.24 \text{ eV (95\% CL, no prior on } B). \end{aligned}$$

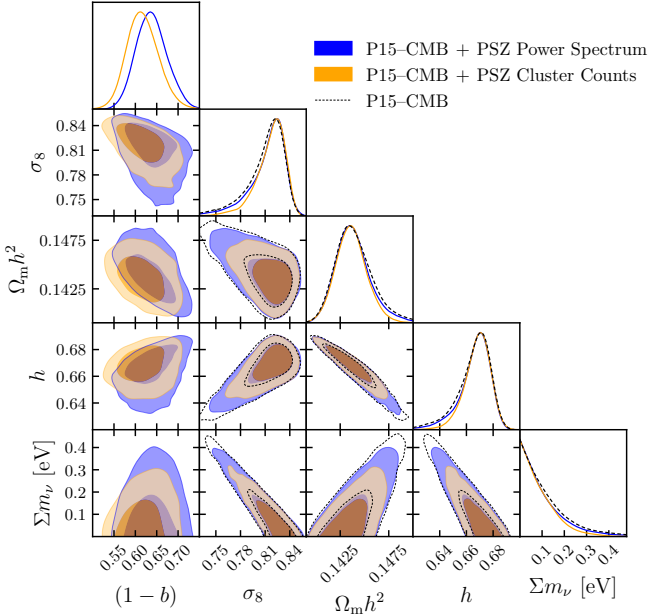


Figure 6. Marginalised (1d and 2d) joint posterior probability distributions with 68% CL and 95% CL contours (for a sub-set of parameters) obtained from the Planck y -map power spectrum (blue) and Planck SZ cluster counts (orange) combined with Planck 2015 primary CMB in $\nu\Lambda$ CDM. Contours from Planck 2015 primary CMB alone are the dashed lines.

With Planck y -map power spectrum we obtain

$$\begin{aligned} F &= 0.469^{+0.004}_{-0.003} & (68\% \text{ CL}), \\ (1-b) &= 0.64^{+0.03}_{-0.04} & (68\% \text{ CL}), \\ \Sigma m_\nu &< 0.32 \text{ eV} & (95\% \text{ CL, no prior on } B). \end{aligned}$$

These results show a remarkable consistency between the Planck SZ cluster counts and y -map power spectrum data: constraints on the X-ray mass bias, F and F^* are consistent with each other at the half- σ level.

However, the resulting values of the X-ray mass bias are not consistent with the HSE value $(1-b) \approx 0.8$. Contours for both analyses, as well as for Planck 2015 primary CMB alone, are shown on Figure 6 for a sub-set of parameters. The marginalised posterior probability distribution for the total neutrino mass does not peak at any particular value.

One could argue that leaving the X-ray mass bias unconstrained is not relevant as this is equivalent to saying that the cluster masses are unknown. We therefore performed analyses where we used the Gaussian prior of Section 5.5 on the bias, i.e., $B = 1.250 \pm 0.125$. The resulting constraints on F^* and F are the same as without the X-ray mass bias prior. Also, like previously, the marginalised posterior probability distribution for the total neutrino mass does not peak at any particular value. However, the $2\text{-}\sigma$ limit of the total neutrino mass becomes weaker. More precisely, with the X-ray mass bias prior, for Planck 2015 primary CMB combined with Planck SZ cluster counts we obtain

$$\begin{aligned} (1-b) &= 0.68^{+0.03}_{-0.04} & (68\% \text{ CL}), \\ \Sigma m_\nu &< 0.37 \text{ eV} & (95\% \text{ CL, prior on } B). \end{aligned}$$

With Planck y -map power spectrum we obtain

$$\begin{aligned} (1-b) &= 0.69 \pm 0.03 & (68\% \text{ CL}), \\ \Sigma m_\nu &< 0.39 \text{ eV} & (95\% \text{ CL, prior on } B). \end{aligned}$$

The 1d posterior probability distribution of the total neutrino mass extends towards larger values when we adopt a Gaussian prior on the X-ray mass bias centred on B_{HSE} , because, in this case, the Planck SZ data is consistent with a matter clustering significantly lower than the one favoured by Planck 2015 primary CMB (see left panel of Figure 5). Hence, a larger neutrino mass helps to bring the primary CMB inferred σ_8 towards lower values, more consistent with the SZ inferred σ_8 . Nevertheless, with our bias prior, the combination of SZ with Planck 2015 primary CMB does not single-out a particular value of the total neutrino mass. On the contrary, we find that the data combination prefers pushing the X-ray mass bias to the upper end of the Gaussian prior, rather than increasing the neutrino mass. We summarised our results on the X-ray mass bias from Planck SZ plus Planck 2015 primary CMB in the right panel of Figure 5 along with several other constraints from weak lensing cluster mass calibrations.

5.7 Planck SZ with Planck 2015 primary CMB and BAO

In $\nu\Lambda$ CDM, for Planck 2015 primary CMB combined with BAO we find $\Sigma m_\nu < 0.134 \text{ eV}$ (95% CL). This is consistent with the results of Alam et al. (2017), i.e., $\Sigma m_\nu < 0.16 \text{ eV}$ (95% CL), although slightly stronger because we use a prior on τ rather than the ‘lowP’ likelihood.¹² When we do not use a prior constraint on the X-ray mass bias, the addition of Planck SZ improves the $2\text{-}\sigma$ limit only by a few percent. More precisely, with Planck SZ cluster counts we obtain

$$\Sigma m_\nu < 0.129 \text{ eV} \text{ (95\% CL, no prior on } B),$$

and with Planck y -map power spectrum we obtain

$$\Sigma m_\nu < 0.127 \text{ eV} \text{ (95\% CL, no prior on } B).$$

Like in the previous section, with a Gaussian prior on the X-ray mass bias, the addition of SZ to Planck 2015 primary CMB and BAO slightly degrades the $2\text{-}\sigma$ limit on the total neutrino mass. Indeed, when we use the Gaussian prior on the X-ray mass bias of Section 5.5, we obtain

$$\Sigma m_\nu < 0.164 \text{ eV} \text{ (95\% CL, prior on } B)$$

with Planck SZ cluster counts and

$$\Sigma m_\nu < 0.149 \text{ eV} \text{ (95\% CL, prior on } B)$$

with Planck y -map power spectrum. Again, we do not find that the marginalised posterior probability distribution of the total neutrino mass peaks at a particular value in any of these analyses. Regarding the X-ray mass bias, we obtain the same constraints as in the previous section at the half- σ level, i.e., using Planck SZ plus Planck 2015 primary CMB.

¹² Low- ℓ polarisation TE,EE,BB likelihood.

5.8 Massive neutrinos and dark energy

Before presenting the joint constraints from Planck SZ with CMB and BAO data in νw CDM, we update the analysis of Bolliet et al. (2018), i.e., the measurement of the equation of state of dark energy from the Planck y -map power spectrum by using only minimal information from primary CMB consisting of a normalisation prior on $A_s e^{-2\tau}$, as well as the prior on the optical depth τ , complemented by a measurement of the Hubble constant.

Once H_0 is fixed, a correlation between w and the angular size of the sound horizon at decoupling arises. Hence, the prior on θ_s used in Bolliet et al. (2018) is crucial for the measurement of w . But since the Planck 2015 primary CMB constraint on θ_s is model-independent, i.e., it is essentially the same in models with dark energy or massive neutrinos (see Table 5 of Planck Collaboration 2018), we can use this information to improve the constraint. We consider the latest measurement of the Hubble constant from Riess et al. (2019) and use a Gaussian prior on the X-ray mass bias, $B = 1.410 \pm 0.141$ corresponding to $(1 - b) \approx 0.7$, consistent with the results of our joint analyses of Planck 2015 primary CMB with Planck SZ with constrained bias and also with Zubeldia & Challinor (2019). In Table 3, we report the priors and external measurements for this analysis.

In Λ CDM with $\Sigma m_\nu = 0.06$ eV, we obtain the constraint $w = -1.22^{+0.10}_{-0.08}$ (68% CL) from the analysis of the Planck y -map power spectrum. We note that the mean value depends on our choices of X-ray mass bias and Hubble constant. For instance, a smaller bias B , or a smaller H_0 , would drive w towards less-negative values. The same method can be applied to find a constraint on the total neutrino mass. In $\nu\Lambda$ CDM ($w = -1$) with the same settings we find $\Sigma m_\nu < 0.17$ eV (95% CL), almost the same as with full CMB information. However, in νw CDM we note that this method does not allow for a constraint on either of these parameters because of the degeneracy between w and Σm_ν : the effects of a more-negative w can be compensated by more-massive neutrinos.

Due to this degeneracy, when we do the same analyses as in the previous section (combining Planck SZ cluster counts or Planck y -map power spectrum with Planck 2015 primary CMB, BAO data and with the Gaussian prior on the X-ray mass bias around B_{HSE}) in νw CDM, the $2\text{-}\sigma$ limit on the total neutrino mass becomes significantly weaker than in $\nu\Lambda$ CDM (see Section 5.7). More precisely, with Planck y -map power spectrum we obtain

$$\begin{aligned} \Sigma m_\nu &< 0.28 & (95\% \text{ CL}), \\ w &= -1.07^{+0.09}_{-0.06} & (68\% \text{ CL}), \end{aligned}$$

and with Planck SZ cluster counts we obtain

$$\begin{aligned} \Sigma m_\nu &< 0.32 & (95\% \text{ CL}), \\ w &= -1.09^{+0.10}_{-0.07} & (68\% \text{ CL}). \end{aligned}$$

For the X-ray mass bias, we obtain the same constraints as in Section 5.6 at the half- σ level, i.e., using Planck SZ plus Planck 2015 primary CMB with Gaussian prior on B .

	mean $\pm \sigma$
$10^9 A_s e^{-2\tau}$	1.878 ± 0.014
τ	0.06 ± 0.01
h	0.7403 ± 0.0142
$100\theta_s$	1.04093 ± 0.00030
B	1.410 ± 0.141

Table 3. Gaussian priors for the analyses of Section 5.8. The normalisation prior is the one derived in Bolliet et al. (2018), the τ prior is from Calabrese et al. (2017b), the h prior is from Riess et al. (2019), the θ_s prior is the same as in Zubeldia & Challinor (2019). The X-ray mass bias prior is motivated by the results of Section 5.6, and those of Zubeldia & Challinor (2019).

6 FORECASTS

To assess the constraining power of cosmic variance limited SZ power spectrum measurements we use the MCMC method, expected to be more reliable and accurate than the Fisher matrix method (e.g., Perotto et al. 2006, for a comparison of both methods). We describe the settings of our analyses in Section 6.1 and present our results in Section 6.2.

6.1 Analyses settings

To generate realistic mock SZ power spectrum data one should in principle draw the SZ power spectrum data points from the n -point probability distribution function of the SZ power spectrum (where n is the number of multipole bins). Zhang & Sheth (2007) presented the theoretical framework to compute it. They explained that the evaluation of the probability distribution function when n is large requires sophisticated Monte-Carlo integration methods, but that for a large sky coverage at sufficiently large ℓ the probability distribution function is well approximated by a multivariate Gaussian distribution. Hence, we bin our mock data from $\ell_{\min} = 200$ to $\ell_{\max} = 10^3$, or 10^4 , with constant logarithmic bin width $\Delta \ln \ell = 0.3$ and use the same sky fraction as the Planck y -map, i.e., $f_{\text{sky}} = 0.47$. Then, to random draw the mock data we use the Cholesky decomposition of the covariance matrix, i.e., $M = LL^t$ where L is a lower triangular matrix with positive diagonal elements. So that the mock power spectrum is given by $\tilde{C}_\ell = C_\ell^{\text{mock}} + s_\ell$ where C_ℓ^{mock} is the SZ power spectrum calculated for the the fiducial model, and $\mathbf{s} = L\mathbf{v}$ with \mathbf{v} a vector of n random numbers drawn from the Normal distribution.

For the fiducial model we use the Planck 2018 cosmological parameters (fifth column of Table 2 of Planck Collaboration 2018) with a total neutrino mass $\Sigma m_\nu = 0.06$ eV and a reference bias $B = 1.41$. On the top panel of Figure 7 we show our mock SZ power spectrum data. In this figure, in particular at large angular scales ($\ell < 10^3$), we can see a multipole-to-multipole correlation between the mock SZ data points which is due to the large non-Gaussian contributions to the covariance matrix (trispectrum). Since masking the heaviest halos increases the signal-to-noise (see bottom panel of Figure 7), we considered two upper bounds for the mass integration, namely $M_{\max} = 5 \times 10^{14} M_\odot / h$ (masking) and $M_{\max} = 5 \times 10^{15} M_\odot / h$ (no masking).

Kodwani et al. (2018) argued that using a fixed covariance matrix is generally more consistent than using a covariance that varies at each steps of the MCMC. In the MCMC analysis, we therefore use a fixed covariance matrix,

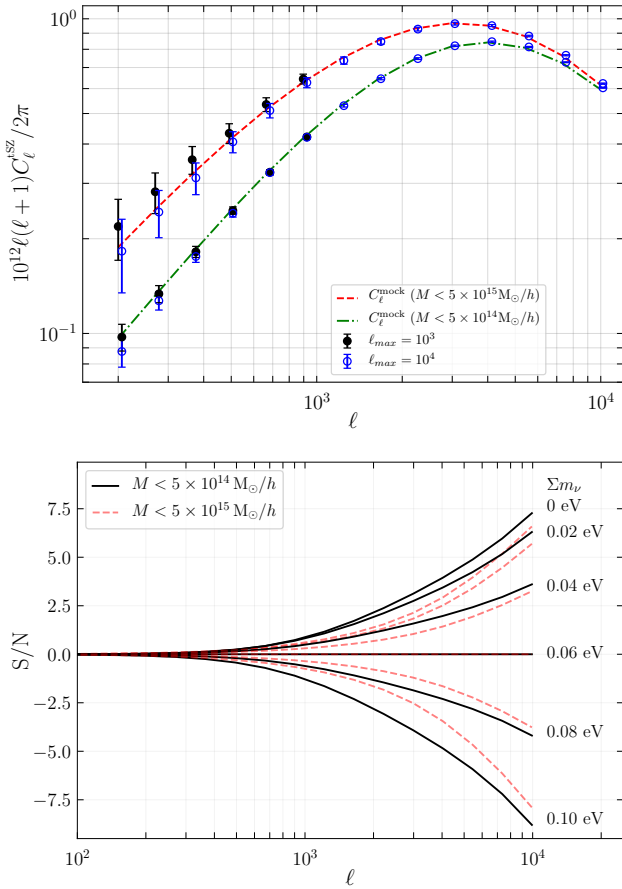


Figure 7. (Top panel) Mock SZ power spectra with error bars for $\ell_{\text{max}} = 10^3$ and $\ell_{\text{max}} = 10^4$, and the models used to compute them (Planck 2018 cosmology and X-ray mass bias $B = 1.41$) for two different values of M_{max} . (Bottom panel) Variation of signal-to-noise ‘S/N’ with respect to a fiducial total neutrino mass at $\Sigma m_\nu = 0.06$ eV for two different values of M_{max} . Note that we use $f_{\text{sky}} = 0.47$.

with Gaussian and non-Gaussian (trispectrum) contribution computed with the parameters of the fiducial model.¹³

To obtain competitive constraints on the neutrino masses, it is necessary to combine the SZ power spectrum with CMB and potentially BAO data. For the CMB we use a combination of a mock Planck and a mock CMB-S4 likelihood from Brinckmann et al. (2019), with mock Planck comparable in sensitivity to the final Planck release Planck Collaboration (2018) and CMB-S4 specifications from Abazajian et al. (2016). The mock CMB combination is only temperature and polarisation (i.e., no lensing power spectrum) and consists of Planck up to $\ell \leq 50$ at 57% sky fraction, CMB-S4 at $50 < \ell < 3000$ with 40% sky coverage plus Planck with 17% sky coverage (intended to avoid regions of overlapping data). See Brinckmann et al. (2019) for more details on the likelihoods. For BAO we use a mock DESI likelihood as

in Archidiacono et al. (2017) with redshifts $0.15 < z < 1.85$ known at percent level precision (Font-Ribera et al. 2014; Allison et al. 2015). We emphasise that in combination with the mock SZ power spectrum we use the ‘2pt’ CMB information, i.e., without the lensing power spectrum (‘4pt’). Nevertheless, for comparison, we also quote the ‘4pt’ CMB-S4 constraint.

6.2 Forecasted constraints

For Planck plus CMB-S4, the sensitivity does not enable a determination of Σm_ν with statistical significance but an upper bound: $\Sigma m_\nu < 0.18$ eV (95% CL). For Planck plus CMB-S4 with lensing power spectrum we obtain $\Sigma m_\nu < 0.16$ eV (95% CL). When we combine Planck plus CMB-S4 with BAO we find a determination of the total neutrino mass with $\sigma(\Sigma m_\nu)^{2\text{pt}} = 28$ meV. The addition of lensing power spectrum to CMB and BAO yields $\sigma(\Sigma m_\nu)^{4\text{pt}} = 25$ meV, consistent with published CMB-S4 forecasted constraints (Abazajian et al. 2016; Brinckmann et al. 2019) as well as the Simons Collaboration (2018) goals.

For mock SZ power spectrum with Planck plus CMB-S4, we obtain an improvement on the total-neutrino mass constraints over Planck plus CMB-S4 in the following cases. With mock SZ power spectrum up to $\ell_{\text{max}} = 10^3$, a 1% prior on the X-ray mass bias and masking, we obtain $\Sigma m_\nu < 0.16$ eV (95% CL). With $\ell_{\text{max}} = 10^4$, we obtain

$$\sigma(\Sigma m_\nu) = 31 \text{ meV} (\ell_{\text{max}} = 10^4, \text{ masking, } 10\% \text{ prior on } B),$$

$$\sigma(\Sigma m_\nu) = 29 \text{ meV} (\ell_{\text{max}} = 10^4, \text{ masking, } 1\% \text{ prior on } B).$$

Contours for the latter analysis and a sub-set of parameters are shown on Figure 8 along with Planck plus CMB-S4 and Planck plus CMB-S4 with BAO contours. Note that our forecasted sensitivity to the optical depth mainly comes from our mock low- ℓ TE,EE polarisation data yielding $\sigma(\tau) = 0.004$, slightly stronger than the final Planck Collaboration (2018) constraint but weaker than the CLASS experiment projected sensitivity (Watts et al. 2018).

For mock SZ power spectrum with CMB and BAO, we obtain an improvement of the total-neutrino mass constraints upon CMB plus BAO when we use $\ell_{\text{max}} = 10^4$. In this case, the analyses with the 1% and 10% priors on the X-ray mass bias give the same results. Without masking we obtain

$$\sigma(\Sigma m_\nu) = 26 \text{ meV} (\ell_{\text{max}} = 10^4, \text{ no masking, BAO}).$$

With masking we obtain

$$\sigma(\Sigma m_\nu) = 24 \text{ meV} (\ell_{\text{max}} = 10^4, \text{ masking, BAO}),$$

i.e., a $\approx 14\%$ improvement over CMB plus BAO, and competitive with the Planck plus CMB-S4 forecast including the lensing power spectrum.

For $\ell_{\text{max}} = 10^4$, we find that the precision on the X-ray mass bias does not affect the total neutrino mass constraint when we combine with Planck plus CMB-S4 and BAO. This is because once the amplitude of primordial curvature perturbations is fixed, the effect of neutrino mass on the SZ power spectrum at small scales differs from the effect at large scales, whereas the effect of the bias is close to a scale-invariant shift of the amplitude. Hence, with $\ell_{\text{max}} = 10^4$, the X-ray mass bias and total neutrino mass are no longer as degenerate as for $\ell_{\text{max}} = 10^3$.

¹³ In principle, one should also follow this for the Planck y -map power spectrum analysis of the previous section. We checked that this difference in methodology does not yield significant changes in the parameter estimation: within a few percent, consistent with Kodwani et al. (2018).

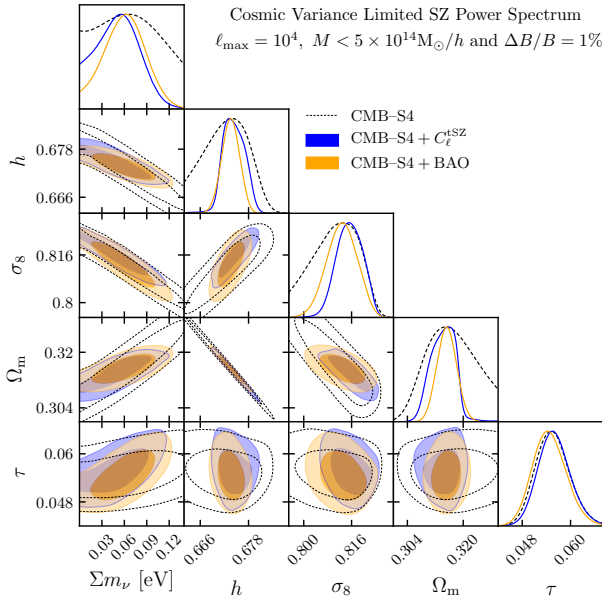


Figure 8. Marginalised (1d and 2d) joint posterior probability distributions with 68% CL and 95% CL contours (for a sub-set of parameters) obtained from the mock cosmic variance limited SZ power spectrum combined with CMB-S4 in $\nu\Lambda$ CDM (blue). The X-ray mass bias is constrained with a Gaussian prior $B = 1.41 \pm 0.014$. Contours for CMB-S4 alone are the dashed lines. Contours for CMB-S4 plus DESI-BAO are in orange. Note that CMB-S4 also includes Planck as described in the last paragraph of Section 6.1, and does not include lensing power spectrum.

We recall that the small-scale SZ power spectrum depends on the details of the ICM pressure profiles, that are not yet fully understood and measured (e.g., [Efstathiou & Migliaccio 2012](#); [Ruppin et al. 2019](#)). Nevertheless, it appears that combining SZ power spectrum with CMB, in the same way as we did here, can yield tight constraints on ICM properties. With our analyses, we can quantify this at the level of the X-ray mass bias parameter. Using mock Planck plus CMB-S4 and cosmic variance limited SZ power spectrum with $\ell_{\max} = 10^3$ and the 10% precision X-ray mass bias prior, we recover the fiducial X-ray mass bias value with $\sigma(B)/B = 1.9\%$ without masking and $\sigma(B)/B = 1.6\%$ with masking. This reduces to $\sigma(B)/B = 1.2\%$ with $\ell_{\max} = 10^4$ and masking. Thus, although it appears challenging to use the SZ power spectrum as an independent cosmological probe of the total neutrino mass, we can safely say that the future of the SZ power spectrum as a probe of the ICM properties is bright.

7 DISCUSSION AND CONCLUSIONS

In this work, we have consistently included the effect of massive neutrinos into the theoretical models for the SZ power spectrum and cluster counts, in line with the works of [Ichiki & Takada \(2012\)](#), [Costanzi et al. \(2013\)](#) and [LoVerde \(2014\)](#). We identified parameter combinations that minimise the relative uncertainty for both the SZ power spectrum analysis and the cluster counts analysis of the Planck SZ data. Explicitly, these are $F_{\text{cb}} \equiv \sigma_8^{\text{cb}}(\Omega_{\text{cb}}/B)^{0.4}h^{-0.2}$ for the

Planck y -map power spectrum and $F_{\text{cb}}^* \equiv \sigma_8^{\text{cb}}(\Omega_{\text{cb}}/B)^{0.35}$ for the Planck SZ cluster counts, where σ_8^{cb} indicates that σ_8 is computed with the power spectrum of CDM and baryons rather than with the total matter power spectrum. For neutrino masses $\Sigma m_\nu \lesssim 1.5$ eV we found that these ‘cb’ parameters are not correlated with the total neutrino mass. In Λ CDM, we obtained the tight constraints $F_{\text{cb}} = 0.456 \pm 0.013$ (68%CL) from the Planck y -map power spectrum alone and $F_{\text{cb}}^* = 0.461 \pm 0.007$ (68%CL) from the Planck SZ cluster counts alone.

In Λ CDM, we fixed the X-ray mass bias to its expected value from hydrostatic equilibrium with a 10% precision Gaussian prior, i.e., $B = 1.250 \pm 0.125$, and obtained constraints on $S_8 \equiv \sigma_8(\Omega_m/0.3)^{0.5}$, $S_8^{0.2} \equiv \sigma_8(\Omega_m/0.3)^{0.2}$, and $S_8^{0.4}h_{70}^{-0.2} \equiv \sigma_8(\Omega_m/0.3)^{0.4}h_{70}^{-0.2}$ from the Planck cluster counts and Planck y -map power spectrum analyses in Λ CDM (see Figure 4). We found that the Planck SZ constraints are consistent with results from SPT-SZ, KiDS+VIKING-450 and DES-Y1 and in mild tension with Planck 2015 primary CMB.

In $\nu\Lambda$ CDM, when we leave the X-ray mass bias free and combine the Planck SZ data with the Planck 2015 primary CMB data, we obtained constraints on the X-ray mass bias that are not consistent with the hydrostatic equilibrium expectation. From Planck 2015 primary CMB with Planck y -map power spectrum, we obtained $(1-b) = 0.64^{+0.03}_{-0.04}$ (68%CL), and with Planck cluster counts we obtained $(1-b) = 0.62^{+0.03}_{-0.04}$ (68%CL). These values agree within $1-\sigma$ with other published results (e.g., [Planck Collaboration 2016c](#); [Makiya et al. 2018](#); [Salvati et al. 2018](#)). We found that the addition of the SZ data to Planck 2015 primary CMB improves the neutrino mass constraint marginally. Our strongest constraint is with SZ cluster counts, namely $\Sigma m_\nu < 0.24$ eV (95%CL). Nevertheless, if we set a Gaussian prior on the bias, the total neutrino mass constraint becomes weaker (see last paragraph of Section 5.6). The same is true when we combine Planck SZ data with CMB and BAO (see Section 5.7).

We carried out analyses of the Planck SZ data combined with Planck primary CMB and BAO in νw CDM (Section 5.8) with Gaussian prior on the X-ray mass bias centred around the HSE value. Our results suggest that this combination of data prefers to adjust the X-ray mass bias to the higher end of the Gaussian prior, rather than increasing the total neutrino mass or decreasing w , to accommodate the SZ data with primary CMB.¹⁴ Our results suggest that the apparent tension between Planck SZ data and Planck 2015 primary CMB should be solved by a X-ray mass bias larger than the HSE value, consistent with the one recently obtained from the CMB lensing calibration of the Planck SZ clusters in the analysis of [Zubeldia & Challinor \(2019\)](#) (see right panel of our Figure 5 for a summary of the constraints on the X-ray mass bias). For instance, a larger X-ray mass bias could be explained by the expected departure from HSE of $\approx 20\%$ plus X-ray temperature calibration bias of $\approx 15\%$ for the most massive clusters (see the detailed review by [Pratt et al.](#)

¹⁴ We note that it is only when the X-ray mass bias is *fixed* to the HSE value that we recover a preference for a total neutrino mass around $\Sigma m_\nu = 0.4$ eV, as was obtained by [McCarthy et al. \(2018\)](#).

2019, for a thorough description of current issues related to the cluster mass scale). Given current uncertainties on the X-ray mass bias, this appears as a better solution rather than extending the standard cosmological model. Nevertheless, adjusting the X-ray mass bias would not explain why other recent results from SZ clusters and galaxy surveys have also reported a low matter clustering amplitude compared to primary CMB (see left panel of Figure 5). Hence, extensions to the minimal Λ CDM cosmology are still worth exploring, especially if they can also explain the difference between local measurements of the Hubble constant (e.g., [Riess et al. 2019](#)) and those obtained from Planck primary CMB ([Planck Collaboration 2018](#)). Three examples of such extensions are the local void idea (e.g., [Ichiki et al. 2016](#)), interacting dark matter-dark radiation (e.g., [Buen-Abad et al. 2018](#)) and self-interacting neutrinos (e.g., [Kreisch et al. 2019](#)).

To explore the constraining power of the SZ power spectrum we used mock cosmic variance limited SZ power spectrum experiments up to $\ell_{\max} = 10^3$ and $\ell_{\max} = 10^4$. We found that to improve upon the neutrino mass constraint from Planck plus CMB-S4 combined with DESI-BAO, it is necessary to measure the small-scale power spectrum up to $\ell_{\max} = 10^4$ and mask the the heaviest clusters. For the combination of SZ power spectrum with Planck plus CMB-S4 without BAO, we found that to reach a constraint on total neutrino mass competitive with Planck plus CMB-S4 plus DESI-BAO, a 1% precision on the mass calibration is required. [Louis & Alonso \(2017\)](#) have shown that this level of precision can be achieved using CMB-S4 weak lensing masses. We also note that [Zubeldia & Challinor \(2019\)](#) already obtained a $\approx 10\%$ precision on the X-ray mass bias using Planck SZ cluster and Planck weak lensing data.

The SZ power spectrum at small scales is not only determined by cosmological expansion and perturbations but also by the details of the ICM via the pressure profile. Hence, it may be challenging to use the SZ power spectrum up to $\ell_{\max} = 10^4$ as an independent probe of the total neutrino mass. However, the small-scale SZ power spectrum can instead be used as a powerful probe of the ICM's properties: our mock cosmic variance limited SZ power spectrum experiments easily yield a measurement of the X-ray mass bias at the 2% precision level when we use information from mock Planck plus CMB-S4 experiments to constrain the cosmological parameters. In addition to probing the ICM, other promising avenues for SZ science include the measurement and characterisation of low density regions of our Universe such as filaments between galaxy clusters ([de Graaff et al. 2019](#); [Tanimura et al. 2019](#)) and cosmic voids ([Alonso et al. 2018](#)).

ACKNOWLEDGMENTS

We are especially grateful to Eiichiro Komatsu as well as Colin Hill and Marilena LoVerde for numerous insightful discussions. BB and JC thank the cosmology group at JBCA, and BB also thanks David Alonso, Brad Benson, Ryu Makya, Ian McCarthy for useful interactions relevant to this project. Finally, BB and TB are grateful to Jean-Baptiste Melin, Eunseong Lee and in particular Florian Ruppert for discussions and help with the cluster counts likelihood. We also thank Antony Lewis for providing the publicly available GetDist package that we used for our contour plots.

This work was supported in part by an ERC Consolidator Grant (CMBSPEC), No. 725456 and DOE DE-SC0017848 and the Deutsche Forschungsgemeinschaft through the graduate school Particle and Astroparticle Physics in the Light of the LHC and through the individual grant Cosmological probes of dark matter properties. Simulations for this work were performed with computing resources granted by the RWTH High Performance Computing cluster under project RWTH0113 and by JARA-HPC from RWTH Aachen University under JARA0184. JC was supported by the Royal Society as a Royal Society University Research Fellow at the University of Manchester, UK. This analysis is based on observations obtained with Planck (<http://www.esa.int/Planck>), an ESA science mission with instruments and contributions directly funded by ESA Member States, NASA, and Canada.

REFERENCES

- Abazajian K. N., et al., 2016, arXiv:1610.02743
- Alam S., et al., 2017, *Mon. Not. Roy. Astron. Soc.*, 470, 2617
- Allison R., Caucal P., Calabrese E., Dunkley J., Louis T., 2015, *Phys. Rev.*, D92, 123535
- Alonso D., Hill J. C., Hložek R., Spergel D. N., 2018, *Phys. Rev.*, D97, 063514
- Archidiacono M., Brinckmann T., Lesgourgues J., Poulin V., 2017, *JCAP*, 1702, 052
- Arnaud M., Pratt G. W., Piffaretti R., Böhringer H., Croston J. H., Pointecouteau E., 2010, *A&A*, 517, A92
- Audren B., Lesgourgues J., Benabed K., Prunet S., 2013a, *JCAP*, 2, 001
- Audren B., Lesgourgues J., Bird S., Haehnelt M. G., Viel M., 2013b, *JCAP*, 1301, 026
- Barbosa D., Bartlett J. G., Blanchard A., Oukbir J., 1996, *A&A*, 314, 13
- Bashinsky S., Seljak U., 2004, *Phys. Rev.*, D69, 083002
- Battaglia N., Bond J. R., Pfrommer C., Sievers J. L., 2012, *ApJ*, 758, 74
- Battye R. A., Weller J., 2003, *Phys. Rev. D*, 68, 083506
- Beutler F., et al., 2011, *Mon. Not. Roy. Astron. Soc.*, 416, 3017
- Birkinshaw M., Gull S. F., Hardebeck H., 1984, *Nature*, 309, 34 EP
- Blas D., Lesgourgues J., Tram T., 2011, *JCAP*, 7, 034
- Bleem L. E., et al., 2015, *Astrophys. J. Suppl.*, 216, 27
- Bocquet S., Saro A., Dolag K., Mohr J. J., 2016, *Mon. Not. Roy. Astron. Soc.*, 456, 2361
- Bocquet S., et al., 2018, arXiv:1812.01679
- Bolliet B., Comis B., Komatsu E., Macías-Pérez J. F., 2018, *Monthly Notices of the Royal Astronomical Society*, 477, 4957
- Boyle A., 2019, *JCAP*, 1904, 038
- Boyle A., Komatsu E., 2018, *JCAP*, 1803, 035
- Brinckmann T., Lesgourgues J., 2018, arXiv:1804.07261
- Brinckmann T., Hooper D. C., Archidiacono M., Lesgourgues J., Sprenger T., 2019, *JCAP*, 1901, 059
- Buen-Abad M. A., Schmaltz M., Lesgourgues J., Brinckmann T., 2018, *JCAP*, 1801, 008
- Burenin R. A., Vikhlinin A., Hornstrup A., Ebeling H., Quintana H., Mescheryakov A., 2007, *Astrophys. J. Suppl.*, 172, 561
- Calabrese E., Alonso D., Dunkley J., 2017a, *Phys. Rev.*, D95, 063504
- Calabrese E., et al., 2017b, *Phys. Rev.*, D95, 063525
- Carlstrom J. E., Holder G. P., Reese E. D., 2002, *Ann. Rev. Astron. Astrophys.*, 40, 643
- Cooray A., Sheth R. K., 2002, *Phys. Rept.*, 372, 1
- Costanzi M., Villaescusa-Navarro F., Viel M., Xia J.-Q., Borgani S., Castorina E., Sefusatti E., 2013, *JCAP*, 1312, 012
- Cuesta A. J., Niro V., Verde L., 2016, *Phys. Dark Univ.*, 13, 77
- DES Collaboration 2018, *Phys. Rev.*, D98, 043526
- Di Valentino E., et al., 2018, *JCAP*, 1804, 017

- Dolag K., Komatsu E., Sunyaev R., 2016, *Mon. Not. Roy. Astron. Soc.*, 463, 1797
- Efstathiou G., Migliaccio M., 2012, *Monthly Notices of the Royal Astronomical Society*, 423, 2492
- Eisenstein D. J., Hu W., 1997, *Astrophys. J.*, 511, 5
- Esteban I., Gonzalez-Garcia M. C., Hernandez-Cabezudo A., Maltoni M., Schwetz T., 2019, *JHEP*, 01, 106
- Font-Ribera A., McDonald P., Mostek N., Reid B. A., Seo H.-J., Slosar A., 2014, *JCAP*, 1405, 023
- George E. M., et al., 2015, *Astrophys. J.*, 799, 177
- Giusarma E., Gerbino M., Mena O., Vagnozzi S., Ho S., Freese K., 2016, *Phys. Rev.*, D94, 083522
- Handley W., Lemos P., 2019, arXiv:1902.04029
- Hannestad S., 2010, *Prog. Part. Nucl. Phys.*, 65, 185
- Hasselfield M., et al., 2013, *JCAP*, 7, 008
- Henson M. A., Barnes D. J., Kay S. T., McCarthy I. G., Schaye J., 2017, *Mon. Not. Roy. Astron. Soc.*, 465, 3361
- Hildebrandt H., et al., 2018, arXiv:1812.06076
- Hill J. C., Pajer E., 2013, *Phys. Rev.*, D88, 063526
- Hill J. C., et al., 2014, arXiv:1411.8004
- Hilton M., et al., 2018, *Astrophys. J. Suppl.*, 235, 20
- Hoekstra H., Herbonnet R., Muzzin A., Babul A., Mahdavi A., Viola M., Cacciato M., 2015, *Mon. Not. Roy. Astron. Soc.*, 449, 685
- Holder G., Haiman Z., Mohr J. J., 2001, *ApJ*, 560, L111
- Horowitz B., Seljak U., 2017, *Mon. Not. Roy. Astron. Soc.*, 469, 394
- Hu W., Eisenstein D. J., 1998, *Astrophys. J.*, 498, 497
- Hu W., Eisenstein D. J., Tegmark M., 1998, *Phys. Rev. Lett.*, 80, 5255
- Hurier G., Lacasa F., 2017, *Astron. Astrophys.*, 604, A71
- Ichiki K., Takada M., 2012, *Phys. Rev.*, D85, 063521
- Ichiki K., Yoo C.-M., Oguri M., 2016, *Phys. Rev.*, D93, 023529
- Kaiser N., 1986, *mnras*, 222, 323
- Kaiser N., 1991, *ApJ*, 383, 104
- Kajita T., 2016, *Rev. Mod. Phys.*, 88, 030501
- Kay S. T., Thomas P. A., Jenkins A., Pearce F. R., 2004, *Mon. Not. Roy. Astron. Soc.*, 355, 1091
- Kodwani D., Alonso D., Ferreira P., 2018,] 10.21105/astro.1811.11584
- Komatsu E., Kitayama T., 1999, *Astrophys. J.*, 526, L1
- Komatsu E., Seljak U., 2002, *Mon. Not. Roy. Astron. Soc.*, 336, 1256
- Kravtsov A. V., Klypin A., Hoffman Y., 2002, *ApJ*, 571, 563
- Kravtsov A. V., Vikhlinin A., Nagai D., 2006, *Astrophys. J.*, 650, 128
- Kreisch C. D., Cyr-Racine F.-Y., Doré O., 2019, arXiv:1902.00534
- Lattanzi M., Gerbino M., 2018, *Front.in Phys.*, 5, 70
- Lau E. T., Kravtsov A. V., Nagai D., 2009, *Astrophys. J.*, 705, 1129
- Lesgourgues J., Pastor S., 2006, *Phys. Rept.*, 429, 307
- Lesgourgues J., Mangano G., Miele G., Pastor S., 2013, *Neutrino Cosmology*. Cambridge University Press
- Lewis A., Bridle S., 2002, *Phys. Rev. D*, 66, 103511
- Liu A., Pritchard J. R., Allison R., Parsons A. R., Seljak U., Sherwin B. D., 2016, *Phys. Rev.*, D93, 043013
- LoVerde M., 2014, *Phys. Rev.*, D90, 083518
- LoVerde M., 2016, *Phys. Rev.*, D93, 103526
- Lorenz C. S., Calabrese E., Alonso D., 2017, *Phys. Rev.*, D96, 043510
- Louis T., Alonso D., 2017, *Phys. Rev.*, D95, 043517
- Lukic Z., Heitmann K., Habib S., Bashinsky S., Ricker P. M., 2007, *Astrophys. J.*, 671, 1160
- Makiya R., Ando S., Komatsu E., 2018, *Monthly Notices of the Royal Astronomical Society*, 480, 3928
- Mangano G., Miele G., Pastor S., Pinto T., Pisanti O., Serpico P. D., 2005, *Nucl. Phys.*, B729, 221
- McCarthy I. G., Bird S., Schaye J., Harnois-Deraps J., Font A. S., Van Waerbeke L., 2018, *Mon. Not. Roy. Astron. Soc.*, 476, 2999
- Medezinski E., et al., 2017, *Publications of the Astronomical Society of Japan*, 70
- Mishra-Sharma S., Alonso D., Dunkley J., 2018, *Phys. Rev.*, D97, 123544
- Mroczkowski T., et al., 2019, *Space Sci. Rev.*, 215, 17
- Nagai D., 2006, *Astrophys. J.*, 650, 538
- Nagai D., Vikhlinin A., Kravtsov A. V., 2007a, *ApJ*, 655, 98
- Nagai D., Kravtsov A. V., Vikhlinin A., 2007b, *ApJ*, 668, 1
- Navarro J. F., Frenk C. S., White S. D. M., 1996, *Astrophys. J.*, 462, 563
- Nelson K., Lau E. T., Nagai D., Rudd D. H., Yu L., 2014, *Astrophys. J.*, 782, 107
- Obuljen A., Castorina E., Villaescusa-Navarro F., Viel M., 2018, *JCAP*, 1805, 004
- Oldengott I. M., Barenboim G., Kahlen S., Salvado J., Schwarz D. J., 2019, *JCAP*, 1904, 049
- Palanque-Delabrouille N., et al., 2015, *JCAP*, 1511, 011
- Peebles P. J. E., Daly R. A., Juszkievicz R., 1989, *ApJ*, 347, 563
- Perotto L., Lesgourgues J., Hannestad S., Tu H., Wong Y. Y. Y., 2006, *JCAP*, 0610, 013
- Planck Collaboration 2013a, *Astron. Astrophys.*, 550, A131
- Planck Collaboration 2013b, *Astron. Astrophys.*, 571, A21
- Planck Collaboration 2014a, *Astron. Astrophys.*, 571, A15
- Planck Collaboration 2014b, *Astron. Astrophys.*, 571, A20
- Planck Collaboration 2015, *Astron. Astrophys.*, 594, A22
- Planck Collaboration 2016a, *Astron. Astrophys.*, 594, A11
- Planck Collaboration 2016b, *Astron. Astrophys.*, 594, A13
- Planck Collaboration 2016c, *Astron. Astrophys.*, 594, A24
- Planck Collaboration 2016d, *Astron. Astrophys.*, 594, A27
- Planck Collaboration 2016e, *Astron. Astrophys.*, 596, A107
- Planck Collaboration 2018
- Pratt G. W., Arnaud M., Biviano A., Eckert D., Ettori S., Nagai D., Okabe N., Reiprich T. H., 2019, *Space Sci. Rev.*, 215, 25
- Reichardt C. L., et al., 2012, *ApJ*, 755, 70
- Remazeilles M., Bolliet B., Rotti A., Chluba J., 2019, *Mon. Not. Roy. Astron. Soc.*, 483, 3459
- Riess A. G., Casertano S., Yuan W., Macri L. M., Scolnic D., 2019
- Roncarelli M., Carbone C., Moscardini L., 2015, *Mon. Not. Roy. Astron. Soc.*, 447, 1761
- Ross A. J., Samushia L., Howlett C., Percival W. J., Burden A., Manera M., 2015, *Mon. Not. Roy. Astron. Soc.*, 449, 835
- Ruppin F., et al., 2018, *A&A*, 615, A112
- Ruppin F., Mayet F., Macías-Pérez J. F., Perotto L., 2019
- Salvati L., Douspis M., Aghanim N., 2018, *Astron. Astrophys.*, 614, A13
- Salvati L., Douspis M., Ritz A., Aghanim N., Babul A., 2019
- Sarazin C. L., 1986, *Rev. Mod. Phys.*, 58, 1
- Shi X., Komatsu E., 2014, *Mon. Not. Roy. Astron. Soc.*, 442, 521
- Shi X., Komatsu E., Nelson K., Nagai D., 2015, *Mon. Not. Roy. Astron. Soc.*, 448, 1020
- Shi X., Komatsu E., Nagai D., Lau E. T., 2016, *Mon. Not. Roy. Astron. Soc.*, 455, 2936
- Simons Collaboration 2018, arXiv:1808.07445
- Smith G. P., et al., 2016, *Mon. Not. Roy. Astron. Soc.*, 456, L74
- Sprenger T., Archidiacono M., Brinckmann T., Clesse S., Lesgourgues J., 2019, *JCAP*, 1902, 047
- Sunyaev R. A., Zeldovich Y. B., 1972, *Comments on Astrophysics and Space Physics*, 4, 173
- Tanimura H., et al., 2019, *Mon. Not. Roy. Astron. Soc.*, 483, 223
- Tinker J. L., Kravtsov A. V., Klypin A., Abazajian K., Warren M. S., Yepes G., Gottlober S., Holz D. E., 2008, *Astrophys. J.*, 688, 709
- Vagnozzi S., Giusarma E., Mena O., Freese K., Gerbino M., Ho S., Lattanzi M., 2017, *Phys. Rev.*, D96, 123503
- Vagnozzi S., Brinckmann T., Archidiacono M., Freese K., Gerbino M., Lesgourgues J., Sprenger T., 2018, *JCAP*, 1809, 001

- Vikhlinin A., Kravtsov A., Forman W., Jones C., Markevitch M., Murray S. S., Van Speybroeck L., 2006, *Astrophys. J.*, 640, 691
- Vikhlinin A., et al., 2009, *Astrophys. J.*, 692, 1033
- Villaescusa-Navarro F., Bull P., Viel M., 2015, *Astrophys. J.*, 814, 146
- Watts D. J., et al., 2018, *Astrophys. J.*, 863, 121
- Weinberg D. H., Mortonson M. J., Eisenstein D. J., Hirata C., Riess A. G., Rozo E., 2013, *Phys. Rept.*, 530, 87
- White S. D. M., Efstathiou G., Frenk C. S., 1993, *MNRAS*, 262, 1023
- Yu B., Knight R. Z., Sherwin B. D., Ferraro S., Knox L., Schmittfull M., 2018, arXiv:1809.02120
- Zeldovich Y. B., Sunyaev R. A., 1969, *Ap&SS*, 4, 301
- Zhang P., Sheth R. K., 2007, *Astrophys. J.*, 671, 14
- Zubeldia Í., Challinor A., 2019, arXiv:1904.07887
- de Graaff A., Cai Y.-C., Heymans C., Peacock J. A., 2019, *Astron. Astrophys.*, 624, A48
- de Haan T., et al., 2016, *ApJ*, 832, 95
- de Salas P. F., Pastor S., 2016, *JCAP*, 1607, 051
- de Salas P. F., Forero D. V., Ternes C. A., Tortola M., Valle J. W. F., 2018, *Phys. Lett.*, B782, 633
- von der Linden A., et al., 2014, *Mon. Not. Roy. Astron. Soc.*, 443, 1973